FIBRILPAINT TARGETS AMYLOID FIBRILS FOR UBIQUITINATION

Françoise A. Dekker[1, 2, 3, #], Júlia Aragonès Pedrola[1, 2, 3, #], Adriana Poza-Rodriguez[1, 2, 3], Guy Mayer[4], Shalini Singh[4], Gobert Heesink[5], Mireille M. A. E. Claessens[5], Assaf Friedler[4], Stefan G. D. Rüdiger[1, 2, 3 *]

[1] Cellular Protein Chemistry, Bijvoet Center for Biomolecular Research, Utrecht University, Padualaan 8, 3584CH Utrecht, The Netherlands.

[2] Science for Life, Utrecht University, Padualaan 8, 3584CH Utrecht, The Netherlands.

[3] Protein Chemistry of Disease, Department of Chemistry, Utrecht University, Padualaan 8, 3584CH Utrecht, The Netherlands

[4] Institute of Chemistry, The Hebrew University of Jerusalem, Edmond J. Safra Campus at Givat Ram, Jerusalem 9190401, Israel.

[5] Nanobiophysics, Faculty of Science and Technology, MESA + Institute for Nanotechnology and Technical Medical Centre, University of Twente, 7500AE Enschede, The Netherlands

Running title: Amyloid ubiquitination

Key words: amyloid, PROTAC, ubiquitination, targeted protein degradation, CHIP, E3 ligase, peptides, Tau , Huntingtin, protein fibrils

FibrilPaint targets amyloid fibrils for ubiquitination

Abstract

Neurodegenerative diseases are characterised by the progressive loss of neuronal tissue, and the accumulation of amyloid fibrils. Currently, there are no therapeutics that remove these amyloids. Targeted protein degradation could be a promising strategy to remove fibrils or oligomeric precursors. This approach requires degraders that specifically recognise amyloid fibrils, preferentially in early stages. Here, we introduce FibrilPaint20 (FP20), a peptide that specifically mediates the ubiquitination of amyloid fibrils. It acts as a PROTAC, containing both of a fibril recognition module and a recruitment motif for the E3 ubiquitin ligase CHIP. Importantly, FP20 does not bind to the functional monomer but exclusively to fibrils. Remarkably, FP20 ubiquitinates a set chemically diverse fibrils, unrelated in sequence and morphology. This includes fibrils of the disease-related proteins of α-synuclein, Aβ, Huntingtin and various Tau species, such as patient-derived fibrils from Alzheimer, Frontotemporal Dementia and Corticobasal Degeneration. This makes FP20 interesting for targeting mixed pathologies. Together, FP20 is an attractive lead compound for targeted protein degradation of amyloid fibrils.

1. Introduction

Neurodegenerative diseases are a group of diseases leading to cognitive decline and motor dysfunction in affected individuals [1]. These are disease such as Alzheimer's Disease (AD) , Parkinson's Disease (PD), and Huntington's Disease (HD) [2-5]. Although symptoms and disease progression differ between these diseases, all lead to the progressive degeneration of neuronal tissue. Removal of aggregates is a potentially an attractive strategy. Recently Leqembi receives FDA approval for therapy for Alzheimer's Disease [6-9]. It is an antibody that removes Aβ amyloid. However, the EMA did not approve it for use in the EU as the benefits do not outweigh the risks. Thus, there is a strong need for drugs that would remove fibrils early in the disease process, are cheaper and have milder side effects [10].

These diseases have a common pathological hallmark: the accumulation of aberrant protein aggregates in the form of amyloid fibrils [11-13]. Amyloid fibrils are characterised by the stacking of multiple monomers into layers by the formation of β sheets. Various proteins have the capacity to adopt such amyloid structure. In AD, β amyloid (Aβ) aggregates extracellularly and Tau intracellularly, but disease progression corresponds to Tau accumulation [13-15]. α-synuclein (αSyn) aggregates intracellularly in PD and Huntingtin (Htt) aggregates both in the cytoplasm and in the nucleus in HD [5, 16-18]. Therefore, an intracellular strategy for therapeutic applications is highly desirable.

In healthy conditions, aberrant protein aggregates can be either refolded or degraded in the cell. However, in disease amyloid fibrils remain within the cell, leading to a failure of the Protein Quality Control (PQC) system [19, 20]. This system consists of a network of molecular chaperones and degradation machineries tasked with maintaining equilibrium in protein synthesis, folding, and degradation [21-23]. Bifunctional degraders can exploit this system to initiate degradation of a problematic protein, a process known as targeted Protein Degradation (TPD) [24-27]. Such as degrader connects the target protein and the degradation machinery by having recognition sites for both. The degradation factor typically targeted is an E3 ubiquitin ligase, such that binding of the degrader of the target protein mediates ubiquitylation and subsequent proteasomal degradation. Such compounds are known as Proteolysis Targeting Chimeras (PROTACs) [26, 27]. The first PROTAC compound in phase III clinical trials for cancer therapy [24, 26-28].

An attractive target for TPD in neurodegenerative diseases are protein fibrils and their precursors. The key challenge to develop degraders for fibrils is the effective recognition of the fibril and their early precursors. Recently, we discovered the Fibril Paint peptides [29], a class of peptides that target multiple amyloid fibrils. Among them,FibrilPaint1 (FP1)[30] is particularly noteworthy as it strongly binding to fibrils and

their earliest precursors, they do not bind to monomers of the aggregating species. This makes FP1 an attractive lead to develop fibril-specific degraders.

FP1 is a fluorescein-labelled 22-amino acid peptide with a unique ability to specifically recognise and target a broad spectrum of amyloid fibrils, of different proteins and with different conformations [30, 31]. FP1 also has a C-terminal EEVD tag, which recruits the TPR domain of the E3 ligase Carboxy-terminus of Hsc70-interacting protein (CHIP) [32, 33]. CHIP is an evolutionary conserved protein and ubiquitous expressed in the CNS [32]. It has a dual function of a co-chaperone to Hsp70 and Hsp90 and an E3 ligase known to ubiquitinate over 94 substrates [25, 34], including Tau [35, 36]. Interestingly, it is present in the disease-affected regions of the AD brain [37].

Here we introduce FibrilPaint20 (FP20), FP1 without fluorescein attached to it, as a PROTAC compound, for the ubiquitination of various protein fibrils through the E3-ligase CHIP. We ubiquitinate amyloid fibrils made of Tau, Huntingtin, αSyn, Aβ fibrils, as well as patient-derived fibrils of AD, Frontotemporal Dementia (FTD), and Corticobasal Degeneration (CBD). We demonstrate the possibility to target and ubiquitinate fibrils unrelated in sequence in structure with one compound.

2. Results

2.1 Ubiquitin transfer through the Ubiquitin System

In our previous work, we developed an application of Flow Induced Dispersion Analysis (FIDA) to monitor fibril length [30]. FIDA determines the size of the fluorescently labelled particles giving as a readout hydrodynamic radius (R_h) [38, 39]. The R_h value is a measure for the apparent size of a molecular complex. The technique relies on the dispersion of particles through a capillary, at the end of which fluorescence is measured by a detector. Small particles disperse less, resulting in a small R_h, while bigger particles disperse more, resulting in large R_h. Ub is a small protein with a predicted R_h* of 1.7 nm. Here we use fluorescently labelled Ub (Fl-Ub) to monitor attachment to various protein and protein complexes. If the small Fl-Ub links to another protein, e.g. an Ub-ligase, this results in a larger fluorescent complex, for which the FIDA can determine the R_h value. As the R_h value can be predicted from structural data (either experimental data or via alphafold predictions), the travelling of Fl-Ub through a cascade of protein with different becomes visible using FIDA.

In fact, we applied this for Fl-Ub for following its passage through the E1, E2 and E3 ligase cascade, which transfers Ub to the degradation target [40, 41] **(Fig. 1A, 1B)**. In this, the Ub-activating enzyme E1 binds Fl-Ub by forming a thioester bond between the glycine residue of Fl-Ub and a cysteine residue on E1, which is a high-energy bond, requiring ATP. Next, Fl-Ub is transferred to the catalytic cysteine residue of Ub-conjugating enzyme E2. Then, E2 interacts with an Ub ligase E3, after which it forms an E2-E3 complex, and Fl-Ub is transferred to the target protein that is bound by the E3.

To reconstitute the Ub cascade, we introduced the E1 (UBE1), E2 (UB2K) and E3 (CHIP) ubiquitin ligases sequentially and we measured the size in FIDA. The R_h gives a direct readout of Fl-Ub binding to these ligases **(Fig 1B)**. The R_h of Fl-Ub was 1.8 nm, in accordance with the predicted R_h* value of 1.7 nm **(Table 1)**. When Fl-Ub bound the Ub-activating enzyme E1 UBE1, we measured an R_h of 6.3 nm, comparable to the predicted R_h* of 5.9 nm. Next, activated Fl-Ub is transferred to the Ub-conjugating enzyme E2 UB2K, which had a predicted R_h* of 3.0 nm, corresponding to 3.4 nm that we measured. Finally, E2 and the Ub ligase E3 interact, resulting in an increase of the R_h, to 4.7 nm. This likely indicates a mixture of specues present, as the CHIP dimer was predicted to have an R_h* of 5.1 nm **(Table 1)**. Passage of Ub through the ligase cascade is ATP dependent. In fact, in absence of ATP, the R_h value remained 1.8 nm, indicating that Fl-Ub did not associate with any of the ligases throughout the experiment. Together, we conclude that we can follow the Fl-Ub transfer through the cascade by tracking the R_h.

Table 1: Used proteins and peptides, used PDB file, predicted hydrodynamic radii (R_h*) and measured hydrodynamic radii (R_h). Predictions based on the PDB file and BioFIDA software R_h predictor.

Protein/Peptide	PDB File	Predicted R_h* (nm)	Measured R_h (nm)
FP1	N/A [30]	1.5	1.7
Ub	1UBQ [42]	1.72	1.8
E1 (UBE1)	AF-P22314-F1 (alphaFold prediction monomer)	4.37	n.a.
E1-Ub (hUBA1-Ub)	6DC6 250kDa [43]	5.85	6.3
E2 (UBE2K/E2-25K)	2BEP [44]	2.32	n.a.
E2-Ub (UBE2K-Ub)	5DFL [45]	2.98	3.4
E3 (CHIP)	2C2L [46]	5.12	n.a.
E2-E3-Ub	n.a.	n.a.	4.7

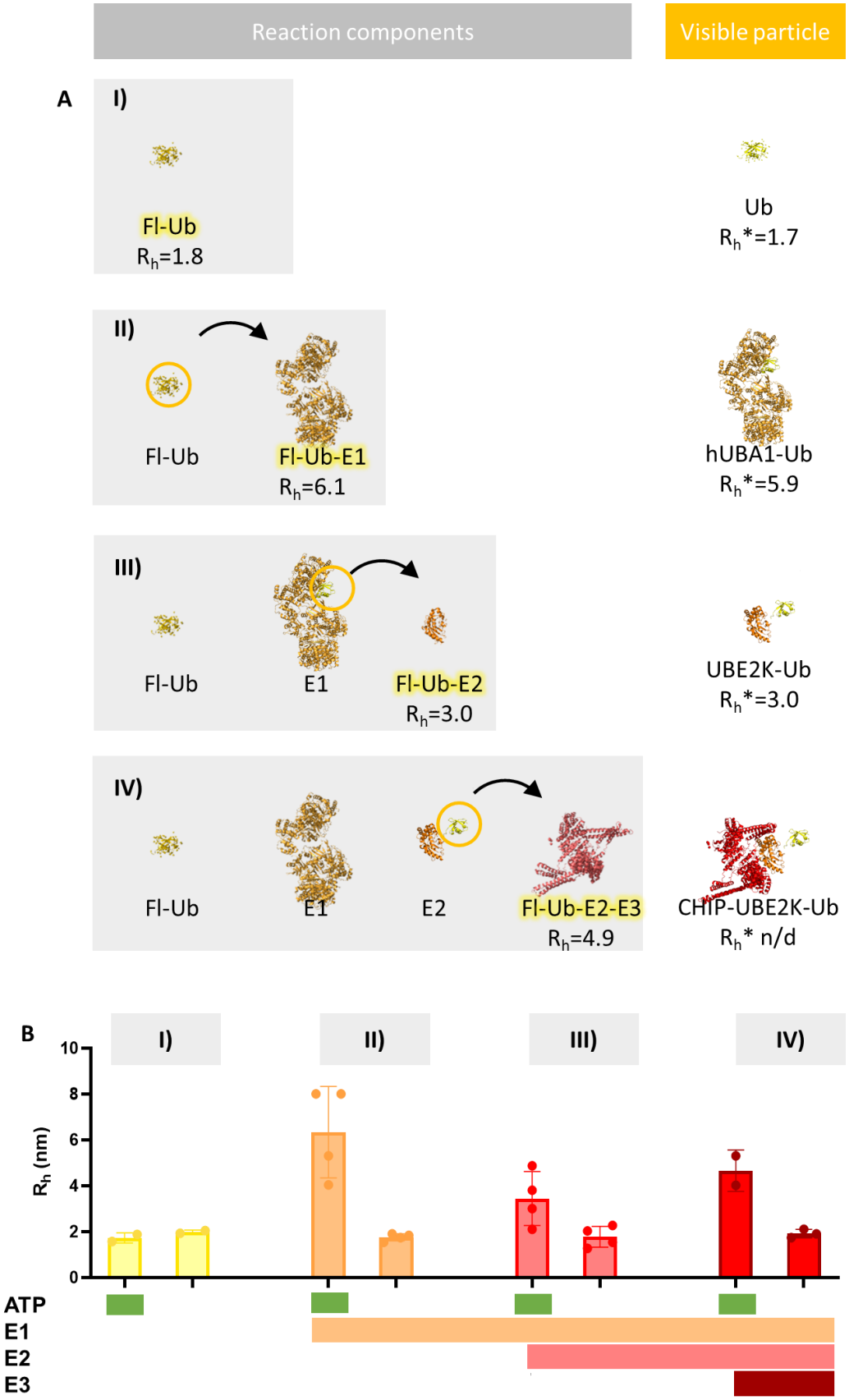
Reaction components
Visible particle
A
I)
Fl-Ub
Rh=1.8
Ub
Rh*=1.7
II)
Fl-Ub
Fl-Ub-E1
Rh=6.1
hUBA1-Ub
Rh*=5.9
III)
Fl-Ub
E1
Fl-Ub-E2
Rh=3.0
UBE2K-Ub
Rh*=3.0
IV)
Fl-Ub
E1
E2
Fl-Ub-E2-E3
Rh=4.9
CHIP-UBE2K-Ub
Rh* n/d
B
I)
II)
III)
IV)
Rh (nm)
0
2
4
6
8
10
ATP
E1
E2
E3

Fig. 1: The ubiquitination cascade. (A) Protein structures of the ubiquitin machinery components present in the reaction mixture, on scale. Transferred particle indicated with yellow circle. Transfer steps indicated with arrow. Measured hydrodynamic radii (R_h) given below end-product of the reaction. Predicted hydrodynamic radii (R_h*), based on available PDB structure, given to the right of the reaction. **I)** Ub only. **II)** Ub binds to an E1 ligase in presence of ATP. **III)** Ub is transferred to an E2 ligase. **IV)** The E3 ligase can recruit the E2 ligase to form an Ub-E2-E3 complex. **(B)** Flow Induced Dispersion Analysis (FIDA) measurement of the ubiquitin machinery reaction products. Present proteins indicated below the graph **I)** Fl-Ubiquitin only, **II)** Fl-Ub-E1, **III)** Fl-Ub-E2, and **IV)** Fl-Ub-E2-E3. Ub, yellow; E1, light orange; E2, dark orange; E3, red. Fluorescent particles indicated with yellow highlight. PDB: Ub, 1UBQ [42], E1, 6DC6 [42]; E2, 2BEP [44]; E3, 2C2L [46].

2.2 FibrilPaint20 binds the E3 ligase CHIP

In a previous study, we demonstrate that FP1 binds amyloid fibrils of unrelated structure and sequence [30]. FP1 has a C-terminal EEVD motif which is a recognition motif to recruit CHIP **(Fig 2A, Table 2)**. To confirm whether FP1 indeed recruits CHIP via the EEVD motif, we titrated CHIP to FP1. FP1 showed a dose-dependent response to higher concentrations of CHIP, with a binding affinity of 1.5 µM **(Fig 2C)**. We repeated the experiment using FP6, a FP1 derivative lacking the C-terminal EEVD motif **(Fig 2A, Table 2)**. FP6 did not bind CHIP **(Fig 2C)**. This demonstes that the EEVD motif is necessary to recruit CHIP to Fibril Paint.

Table 2 – FibrilPaint peptides with corresponding sequences, molecular weight (mw) and predicted R_h. Amino acids are coloured as hydrophobic, yellow; positive charge, blue; negative charge, red.

Peptide	Sequence	mw (kDa)	Predicted R_h (nm)
FibrilPaint1	Fluorescein-PWWRRPWWPWHHPHGSGSEEVD	3.18	1.17
FibrilPaint6	Fluorescein-PWWRRPWWPWHHPH	2.42	1.04
FibrilPaint20	PWWRRPWWPWHHPHGSGSEEVD	2.82	1.11

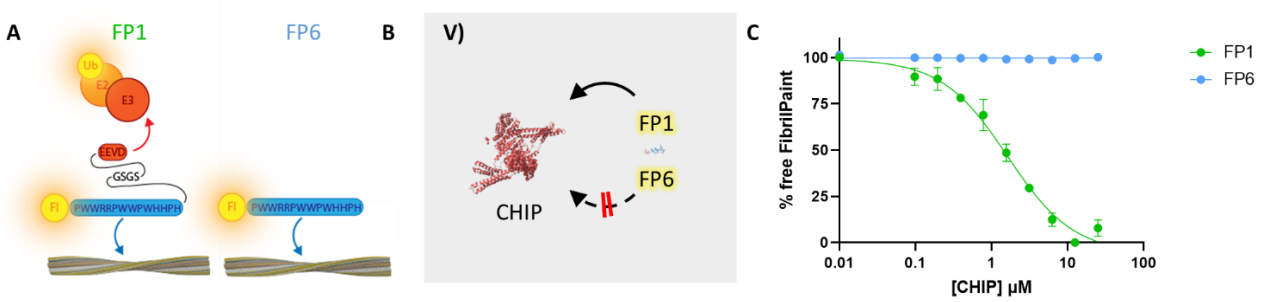

Fig. 2: FibrilPaint1 binds the E3 ligase CHIP. (A) FibrilPaint1 is designed as a PROTAC: the N-terminal side of the peptide binds to amyloid fibrils [30] and the EEVD motif binds to Ub- E3-ligase CHIP, after which the amyloid can be ubiquitinated **(B)** Protein structures available in the reaction mixture, on scale. PDB: E3, 2C2L [46]. **(C)** FibrilPaint1 (green, N=4) binds CHIP with an affinity of 1.5 µM. FibrilPaint6 (blue, N=3) does not bind to CHIP. Ub, yellow; E2, dark orange; E3, red. Fluorescent particles indicated with yellow highlight. FP1 in red and blue, FP6 in blue, same sequence as FP1 but without GSGSEEVD [47]

2.3 FibrilPaint Ubiquitinaties TauRD amyloid fibrils

Next, we aimed to transfer the Fl-Ub to the amyloid fibrils. To achieve it, we used FibrilPaint20 (FP20), which has the same sequence as FP1, but without a fluorescein attached N-terminally **(Table 2)**, preventing interference with the fluorescent signal of Fl-Ub. We used the same ubiquitination system, in presence of recombinant TauRD fibrils as substrate and FP20 to recruit the system to the amyloid fibrils **(Fig 3A)**. TauRD is the repeat domain of the Tau protein, which aggregates in multiple tauopathies, among which AD, the most prevalent neurodegenerative disease [48, 49].

In presence of ATP, the ubiquitin machinery and TauRD amyloid fibrils, the measured R_h increased from 1.8 nm to 42 nm **(Fig. 3B)**. This R_h corresponds to the R_h measured for TauRD fibrils made under similar conditions using FP1 [30], which was 44 nm. This is a typical value for protein fibrils, which also exceeded by far the size of the largest complex observed in the ubiquitin transfer cascade (6.3 nm when bound by E1) **(Fig. 1B)**. Therefore, we conclude that Fl-Ub formed a complex with TauRD fibrils. In absence of ATP, the R_h remained 1.8 nm, which corresponds to the free Fl-Ub.

To confirm that the TauRD fibrils are covalently ubiquitinated, and not only forming a complex with the fibrils, we treated the complex with high cncentrations of urea, which denatures most proteins and protein-protein interactions while protein fibrils remain stable **(Fig 3B)**. After the addition of 4 M urea, the

R_h remained at 42 nm **(Fig. 3B)**. This indicates that Fl-Ub was covalently attached to the fibrils. This demonstartes that FP20 acts as a PROTAC for TauRD fibrils.

2.3 FibrilPaint Ubiquitinaties multiple amyloid fibrils

After establishing the ability of FP20 to ubiquitinate TauRD fibrils, we extend our approach to other amyloids. We used three additional recombinant amyloid fibrils, which are completely different in sequence and structure. HttEx1Q44 is a fragment of Huntingtin, which aggregates in HD if the polyQ repeat exceeds a threshold of at least 36 repeats [5, 50, 51]. αSyn is an 140 aminoacid protein which aggregates in PD and other synucleopathies [16, 52]. Aβ is a peptide that aggregates extracellularly in AD, and preceeds the aggregation of Tau [53-55].

We used the same experimental set-up as for the ubiquitination of TauRD fibrils. We measured an R_h of 62 nm for HttEx1Q44, which shifts to 45 nm after the addition of urea **(Fig. 3C).** This downshift may be related to dissolving bundles off huntingtin fibrils, or to the natural hetergeneous nature of these fibrils [56, 57]. For αsyn the measured R_h was 60 nm, and after the addition of urea the R_h was 61 nm **(Fig. 3D)**. For Aβ we observed an R_h of 73 nm and 75 nm after the addition of urea **(Fig. 3E)**. In absence of ATP, the R_h was 1.8 nm for all conditions, corresponding to the R_h of Fl-Ub only. Together, these data demonstrate the transfer of Fl-Ub to various amyloid fibrils by FP20.

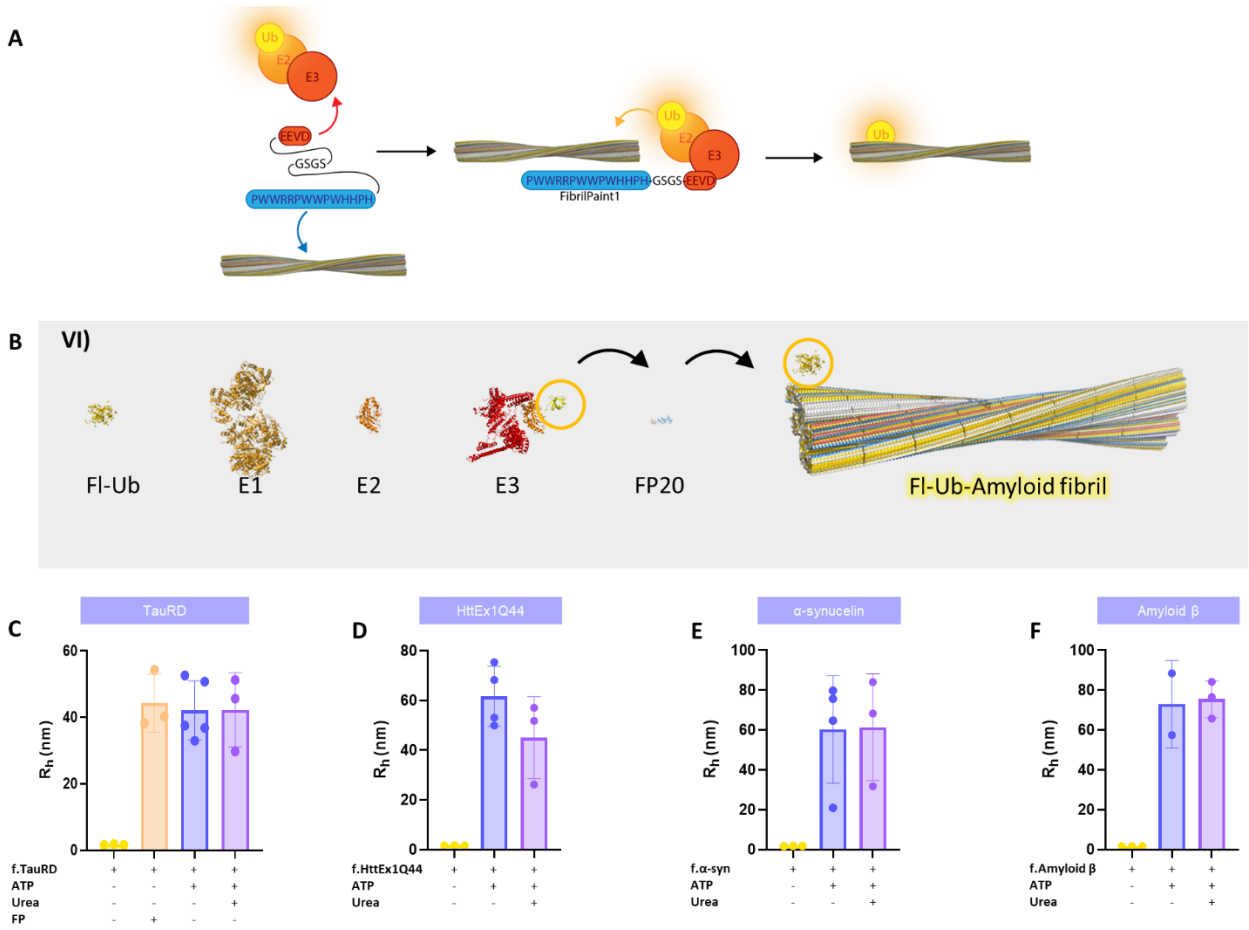

Fig. 3: FibrilPaint20 targets amyloid fibrils for ubiquitination. (A) Schematic of FP20 targeting amyloid fibrils and recruiting the E3 ligase CHIP, after which a complex is formed and the Ub is transferred to the amyloid fibril. **(B)** Protein structures available in the reaction mixture, on scale. PDB: Ub, 1UBQ [42], E1, 6DC6 [42]; E2, 2BEP [44]; E3, 2C2L [46]; fibril based on PHF [58]. Ubiquitination of TauRD **(C)**, HttEX1Q44 **(D)**, α-synuclein **(E)**, and Amyloid β **(F)** in absence of ATP (yellow), in presence of ATP (lilac) and after addition of urea (purple). Ub, yellow; E1, light orange; E2, dark orange; E3, red. Fluorescent particles indicated with yellow highlight. FP20 in red and blue, amyloid fibril with YRB colours [47]. Transferred particle indicated with yellow circle. Transfer steps indicated with arrow.

2.4 FibrilPaint20 ubiquitinates patient-derived fibrils

Having established FP20's ability to act as a PROTAC for the ubiquitination of various recombinant amyloid fibrils, we investigated its capability to ubiquitinate patient-derived amyloid fibrils. Patient-derived fibrils differ from recombinant fibrils conformationally [59]**.** Tau fibrils are particularly interesting as various tauopathies are characterised by distinctive fibril morphologies [48, 60, 61]. AD, Frontotemporal Dementia (FTD) and Cortical Basal Degeneration (CBD) are three Tauopathies in which Tau aggregates into amyloid fibrils. In AD, Tau that aggregates into paired helical filaments (PHF) and Straight Filaments (SF) [58]. In

FTD, Tau forms narrow filaments [62]. In CBD, Tau aggregates in different conformations, into Type I and Type II fibrils [63]. All of these amyloid fibrils, although they are built up from the same protein, have different conformations, and different amino acids exposed and buried in the amyloid core [48]. The differences among conformations can lead to different properties.

We extracted fibrils from patients diagnosed with AD, FTD and CBD [30, 58, 62, 63]. Next, we used FP20, Fl-Ub and the Ubiquitination ligase cascade to ubiquitinate these patient-derived fibrils (**Fig 4A)**. For AD, the R_h was 130 nm (**Fig. 4B)**. For FTD, the R_h was 70 nm (**Fig. 4C F**or CBD, the R_h was 80 nm **(Fig. 4D)**. These values differ to some extent from those for fibrils we have characterised previously [30]. This is not unexpected as these are independent purifications of samples that originate from different brain regions [30]. For all these different Tauopathies, Ub is transferred to the amyloid fibril in presence of FibrilPaint20. Thus, FP20 also mediates the ubiquitination of patient-derived fibrils.

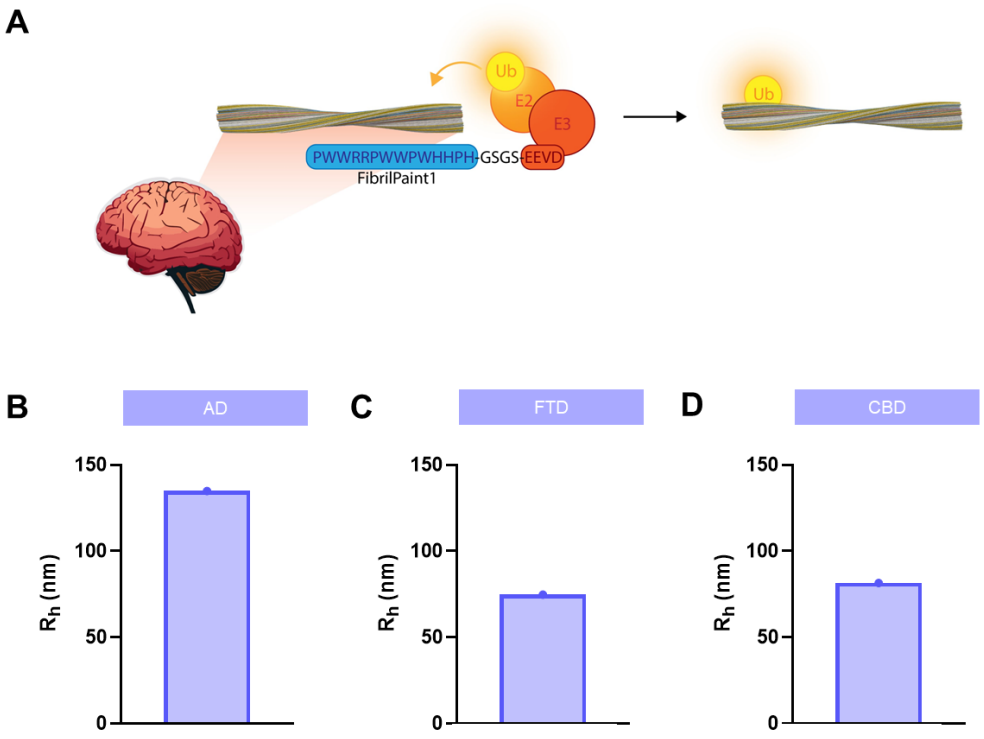

Fig. 4: FibrilPaint20 targets patient-derived amyloid fibrils for ubiquitination. (A) Schematic of patient-derived fibrils, bound by FIbrilPaint to facility the transfer of Ubiquitin by an E3 ligase to covalently label these amyloid fibrils. R_h measured of fluorently-labeled ubiquitin attached to fibrils from Alhzeimer's Disease **(B)** Frontotemporal Dementia **(C)** and Corticobasal degeneration **(D)**.

Together, FP20 covalently ubiquitinates recombinant fibrils of TauRD, HttEx1Q44, αSyn and Aβ **(Fig 3)**. Ubiquitination was not limited to recombinant structures, but could be extended to patient-derived fibrils from AD, CBD and FTD **(Fig 4)**. Hence, we demonstrate the ability to use one compound to target multiple amyloid fibrils. Ubiquitination can be a signal for degradation by the ubiquitin-proteasome system or the autophagic machinery [64] **(Fig. 5)**. Both rely on poly-ubiquitination of the substrate as a signal for degradation, where the lysine coupling on ubiquitin dictates protein fate [65]. Modifying FibrilPaints for their binding by ubiquitin ligases may therefore pose a starting point to therapeutically intervene amyloid build up.

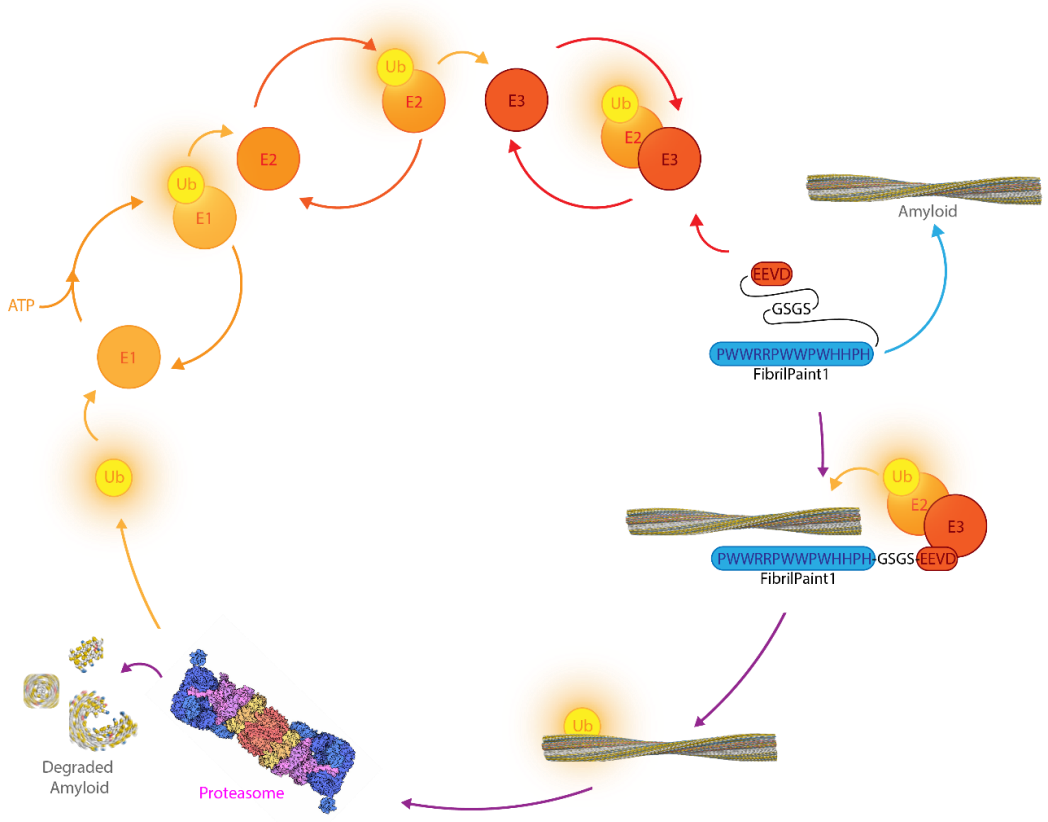

Figure 5: Outlook: FibrilPaint20 targets amyloid fibrils for ubiquitination, which could be used for targeted protein degradation. Ubiquitin goes through an enzymatic cycle of the E1, E2 and E3 ligase in presence of ATP. FibrilPaint20 binds E3, and amyloid fibrils, enabling the transfer of Ub to the amyloid fibril, covalently labelling the amyloid fibril with ubiquitin. Ubiquitin is a cellulular signal, and could be used to signal for proteasomal degradation. Ub, yellow; E1, light orange; E2, dark orange; E3, red. Fluorescent particles indicated with yellow highlight. FP20 in red and blue, amyloid fibril with YRB colours [47]. Transferred particle indicated with yellow circle. Transfer steps indicated with arrow.

3. Discussion

Here we establish FibrilPaint20 as PROTAC compound that specifically ubiquitinates various amyloid fibrils. FP20 mediates ubiquitination of fibrils characteristic of various Tauopathies including AD, FTD and CBD but also chemically entirely unrelated fibrils from PD and HD. Fibrils may either originate from recombinant or primary source, indicating that the specificity is linked to the fibrillic nature itself and not to possible modifications, sequence motifs or disease-specific morphologies.

Targeting the repetitive amyloid structure brings multiple benefits. Recent cryo-EM structures show, the vast structural diversity of amyloids [58, 60-62, 66-69]. It has become clear that in one disease, one could have multiple proteins aggregating, and one protein can end up with multiple conformations [48, 61]. Recently, it has become clear that amyloid structures may also evolve over time [60, 70]. As targeting early is a prerequisite to effective treatment. Thus, the fact that Fibril Paints target a range of structures, including early species, are an important advantage.

Current PROTACs have shown efficient in preventing aggregation by taking out the monomeric precursor [71, 72]. Tau PROTACs are most advanced, often combining a warhead based on a PET tracer with an E3 ligand targeting von Hippel−Lindau (VHL) or Cereblon (CRBN) [71, 73, 74]. Here we introduce the E3 ligase CHIP for a PROTAC strategy. CHIP is attractive as it is the E3 ligase that targets Tau under physiological conditions for degradation [75]. The peptidic recognition motif can be easily added also to other PROTACS, thus its use is not limited to Fibril Paints.

In contrast to other PROTACS, Fibril Paints target fibrils and their early, already fibrillar precursors [30]. This includes stacks of 4-5 layers, but they do not bind to the monomeric precursor [30]. This is a unique and very important advantage of Fibril Paints. An excess of monomers may titrate out fibril paint under physiological conditions. Also removal of a monomer that has important functions in the cell may be problematic and may even proof lethal. For HD specifically, huntingtin PROTACs cannot distinguish between the problematic mutant Htt protein and the the wildtype Htt protein [76, 77]. As wtHtt has important physiological functions the potential of these compounds to reach the clinic is limited [78].

PROTACS need to act under physiological conditions in the cell. As Fibril Paints are peptides, they are intrinsically biocompatible. The sequence is easily adapted to accommodate another strategy, if targeting another E3 would prove more useful. Hundreds of other E3 ligases are available in the body, of which many still have unknown TPD potential [25]. In principle, Fibril Paints could be connected to various E3 ligases or autophagy receptors, since we have shown the sequence of Fibril Paints can be varied [29]. Widely used

E3 ligases for PROTACs include VHL, CBRN, MDM2, DCAF16 and TRIM24 [25]. However, also autophagy can be targeted by strategies such as LYTAC, AUTAC and AUTOTAC [10, 79-84]. This is attractive also for Fibril Paints, as the proteasome is already blocked by larger oligomeric structures [85]. The combination of the stringent specificity for fibrils and their precursors in combination with the adaptability of a peptide sequence make Fibril Paints an attractive lead compounds for TPD of aggregation diseases.

Fibril Paints provide a highly specific and stringent approach to target amyloid fibrils for removal. Remarkably, it is possible to target multiple amyloid fibrils using just one compound. This is a unique and attractive property for a degrader, as a successful development for clinical use could be applied to various pathologies. Targeting various amyloid fibrils may bring additional benefits from a clinical perspective. Clinical diagnosis may differ from found postmortem pathology [86]. In 50% of cases, patients have the pathology of various dementia diseases, varying from 10% to 74% depending on methods used to diagnose [87, 88]. Treatment with a compound that recognises various amyloids may provide a therapeutic strategy, regardless of misdiagnosis or complex pathology.

Fibril Paints are a novel type of protein degraders. They are unique in their specificity for a diverse range of protein fibrils and their earliest precursor. This makes them attractive lead compounds to develop degraders for neurodegeneration.

4. Materials and Methods

Expression and purification of TauRD

We produced N-terminally FLAG-tagged (DYKDDDDK) human TauRD (Q244-E372, with pro-aggregation mutation ΔK280) in E. Coli BL21 Rosetta 2 (Novagen), with an additional removable N-terminal His6-Smt-tag (MGHHHHHHGSDSEVNQEAKPEVKPEVKPETHINLKVSDGSSEIFFKIKKTTPLRRLMEAFAKRQGKEMDSLRFLYDGIRIQADQTPEDLDMEDNDIIEAHREQIGG). Expression was induced at OD600 0.8 by addition of 0.15 mM IPTG and incubation at 18 oC overnight. Cells were harvested by centrifugation, resuspended in 25 mM HEPES-KOH pH=8.5, 50 mM KCl, flash frozen in liquid nitrogen, and kept at – 80 oC until further usage. Pellets were thawed at 37 oC, followed by the addition of ½ tablet/50 ml EDTA-free Protease Inhibitor and 5 mM β-mercaptoethanol. Cells were disrupted using an EmulsiFlex-C5 cell disruptor, and lysate was cleared by centrifugation. Supernatant was filtered using a 0.22 µm polypropylene filtered and purified with an ÄKTA purifier chromatography System. Sample was loaded into a POROS 20MC affinity purification column with 50 mM HEPES-KOH pH 8.5, 50 mM KCl, eluted with a linear gradient 0-100%, 5 CV of 0.5 M imidazole. Fractions of interest were collected, concentrated to 2.5 ml using a buffer concentration column (vivaspin, MWCO 10 KkDda), and desalted using PD-10 desalting column to HEPES pH 8.5, ½ tablet/50 ml Complete protease inhibitor, 5 mM β-mercaptoethanol. The His6-Smt-tag was removed by treating the sample with Ulp1, 4 oC, shaking, overnight. The next day, sample was loaded into POROS 20HS column with HEPES pH 8.5, eluted with 0-100% linear gradient, 12 CV of 1M KCl. Fractions of interest were collected and loaded into a Superdex 26/60, 200 pg size exclusion column with 25 mM HEPES-KOH pH 7.5, 75 mM NaCl, 75 mM KCl. Fractions of interest were concentrated using a concentrator (vivaspin, MWCO 5 kKDda) to desired concentration. Protein concentration was measured using a NanoDrop™ OneC UV/Vis spectrophotometer and purity was assessed by SDS-PAGE. Protein was aliquoted and stored at – 80 oC.

Expression and purification of HttEx1Q44

We produced HttEx1Q44 with in E. Coli BL21 Rosetta 2 (Novagen), with an additional N-terminal MBP- and C-terminal His6-tag (MKIEEGKLVIWINGDKGYNGLAEVGKKFEKDTGIKVTVEHPDKLEEKFPQVAATGDGPDIIFWAHDRFGGYAQSGLLAEITPDKAFQDKLYPFTWDAVRYNGKLIAYPIAVEALSLIYNKDLLPNPPKTWEEIPALDKELKAKGKSALMFNLQEPYFTWPLIAADGGYAFKYENGKYDIKDVGVDNAGAKAGLTFLVDLIKNKHMNADTDYSIAEAAFNKGETAMTINGPWAWSNIDTSKVNYGVTVLPTFKGQPSKPFVGVLSAGINAASPNKELAKEFLENYLLTDEGLEAVNKDKPLGAVALKSYEEELAKDPRIAAT

MENAQKGEIMPNIPQMSAFWYAVRTAVINAASGRQTVDAALAAAQTNAAAASEFSSNNNNNNNNNNLGIEGRMAT LEKLMKAFESLKSFQQQ

a concentrator (vivaspin, MWCO 5 kKDda) to desired concentration. Protein concentration was measured using a NanoDrop™ OneC UV/Vis spectrophotometer and purity was assessed by SDS-PAGE. Protein was aliquoted and stored at – 80 ºC.

Expression and purification of α-synuclein

Human α-synuclein (α-Syn) wild-type was produced recombinantly as described previously (Stöckl et al., 2011). Briefly, protein was produced using the pT7 7 expression system in E. coli BL21 (DE3) cells. After IPTG induction, cells were harvested by centrifugation and resuspended in 10 mM Tris-HCl, PH 8.0, 1 mM EDTA and 1 mM Pefabloc protease inhibitor cocktail. Cells were disrupted by sonication and lysate was cleared by centrifugation. Nucleotides were removed by addition of 1% w/v streptomycin sulphate followed by centrifugation. α-Syn was precipitated by 0.3 g/ml ammonium sulfate and subsequent centrifugation. The pellet was dissolved in 10 mM Tris-HCl, pH 7.4, 1 mM Pefabloc and filtered through a 0.2 µm membrane. Sample was loaded onto a Resource Q anion exchange column (Cytiva) coupled to an ÄKTA purifier chromatography system. Sample was eluted with a salt gradient from 0-1 M. Fractions of interest were collected and desalted with 10 mM Tris-HCl pH 7.4 using a Hiprep 26/10 column (Cytiva). Protein concentration was measured using a NanoDrop UV/Vis spectrophotometer and purity was assessed by SDS-PAGE. Purified protein was aliquoted, flash-frozen with liquid nitrogen and stored in 10 mM Tris-HCl pH 7.4 at -80 °C until further use.

Amyloid-β (1-42) monomer and fibril preparation

Amyloid-beta peptide 1-42 (Aβ42) was purchased from Sigma-Aldrich (A9810). Monomers were solubilized in PBS pH 7.4, according to established protocols (Vandersteen et al., 2012). Aliquots of 10 µM peptide were stored at -20 °C. Monomers were freshly thawed prior to experiments.

Aβ42 fibrils were prepared by quiescent incubation at 37 °C for 20 hours in presence of 0.02 w/v% NaN3. After 4 hours at room temperature (21 °C), we verified the presence of Aβ42 aggregates using AFM. AFM samples were prepared by adsorbing 10 µl of 5 times diluted sample onto mica (Muscovite mica, V 1 quality, EMS) for 45 minutes, after which the mica sheets were carefully washed with milliQ 4 times, covered and left to dry overnight. The Aβ42 fibril samples were stored at room temperature (21 °C).

Peptide synthesis and purification

The peptides were synthesized using a Liberty Blue Microwave-Assisted Peptide Synthesizer (CEM) with standard Fmoc chemistry and Oxyma/DIC as coupling reagents. The peptide concentrations were measured by UV spectroscopy. The peptides were labeled with 5(6)-carboxyfluorescein at their N' termini. The peptides were cleaved from the resin with a mixture of 95% (v/v) trifluoroacetic acid (TFA), 2.5% (v/v) triisopropylsilane (TIS), 2.5% (v/v) triple distilled water (TDW) agitating vigorously for 3 hours at room temperature. The volume was decreased by N2 flux and the peptides precipitated by addition of 4 volumes of diethylether at -20 °C. The peptides were sedimented at -20 °C for 30 minutes, then centrifuged and the diethylether discarded. The peptides were washed three times with diethylether and dried by gentle N2 flux. The solid was dissolved in 1:2 volume ratio of acetonitrile I:TDW, frozen in liquid Nitrogen and lyophilized. The peptides were purified on a WATERS HPLC using a reverse-phase C18 preparative column with a gradient IACN/TDW. The identity and purity of the peptides was verified by ESI mass spectrometry and Merck Hitachi analytical HPLC using a reverse-phase C8 analytical column.

TauRD fibril formation

Aggregation of 20 µM TauRD in 25 mM HEPES-KOH pH 7.4, 75 mM KCl, 75 mM NaCl, ½ tablet/50 ml Protease Inhibitor, was induced by the addition 5 µM of heparin low molecular weight. Aggregation reaction was performed using a thermoshaker 37 °C and 600 rpm during 24 hours.

HttEx1Q44 fibril formation

Aggregation of 20 µM HttEx1Q44 in 25 mM HEPES-KOH pH 7.4, 75 mM KCl, 75 mM NaCl, ½ tablet/50 ml Protease Inhibitor, was induced by the cleavage of C-terminal MBP-tag with Factor Xa. Aggregation reaction was performed using a thermoshaker 37 °C and 600 rpm during 24 hours.

α-Synuclein fibril formation

Monomeric α-Syn was thawed, supplemented with NaCl and NaN_3 and diluted to final concentrations of 50 µM α-Syn, 10 mM Tris-HCl (pH 7.4), 10 mM NaCl and 0.02 w/v% NaN_3. Samples were incubated for 17 days at 37 °C while shaking at 500 rpm. To verify α-Syn aggregation, the samples were centrifuged for 30 minutes at 17000 g. The monomer residual concentration was measured to be 15 µM using UV-Vis absorption (NanoDrop, Thermo Fisher Scientific). The fibrils were resuspended and aliquoted. Fibrils were subsequently stored at room temperature (21 °C).

Fibril extraction

Brain material of FTD and CBD were obtained from the Dutch Brain Bank, project number 1369. Brain material for AD was donated by prof. J. J. M. Hoozemans from the VU Medical Centra Amsterdam.

PHFs and SFs were extracted from grey matter of prefrontal cortex from one patient diagnosed with AD according to established protocols [58]. Tissue was homogenized using a Polytron(PT 2500E, Kinematica AG) on max speed in 20 % (w/v) A68 buffer, consisting of 20 mM TRIS-HCl pH 7.4, 10 mM EDTA, 1.6 M NaCl, 10% sucrose, 1 tablet/10 ml Pierce protease inhibitor, 1 tablet/10 ml phosphatase inhibitor. The homogenized sample was spun from 20 minutes, at 14000 rpm at 4 ^{o}C. Supernatant was collected, and the pellet was homogenized in 10% (w/v) A68 buffer. The homogenized was spun once more. The supernatants of both centrifugations were combined and supplied with 10% w/v Sarkosyl, and incubated for 1 hour on a rocker at room temperature. The sample was ultracentrifuged for 1 hour at 100000xg and 4 ^{o}C. The supernatant was discarded, and the pellet was incubated overnight at 4 ^{o}C in 20 µl/0.2 g starting material of 50 mM TRIS-HCl pH 7.4. The next day, the pellet was diluted up to 1 ml of A68 buffer, and resuspended. To get rid of contamination, the sample was spun for 30 minutes at 14000 rpm, 4 ^{o}C. Supernatant was collected and spun once more for 1 hour at 100000xg, 4 ^{o}C. The pellet was resuspended in 30 µl 25 mM HEPES-KOH pH 7.4, 75 mM KCl, 75 mM NaCl, and stored at 4 ^{o}C up to a month. Presence of PHF and SF was assessed by TEM.

Narrow filaments were extracted from the grey matter of the middle frontal gyrus from one patient diagnosed with FTD (nhb 2017-019), as described in established protocols [62]. Fibrils were extracted following the protocol for AD fibrils. After the first ultracentrifugation step, the pellet was resuspended in 250 µl/1g of starting material of 50 mM Tris pH 7.5, 150 mM NaCl, 0.02% amphipol A8-35. The sample was centrifuged for 30 minutes at 3000xg and 4 ^{o}C. Pellet was discarded, and the supernatant was ultracentrifuged for 1 hour at 100000xg and 4 ^{o}C. The pellet was resuspended in 30 µl of 50 mM TRIS-HCl pH 7.4, 150 mM NaCl, and stored at 4 ^{o}C up to a month. Presence of narrow filaments was assessed by TEM.

CBD fibrils were extracted from the grey matter of the superior parietal gyrus of one patient diagnosed with CBD (nhb 2018-007), following established protocols [63]. Tissue was homogenized using a Polytron(PT 2500E, Kinematica AG) on max speed in 20 % w/v 10 mM TRIS-HCl pH 7.5, 1 mM EGTA, 0.8 M NaCl, 10% sucrose. The homogenate was supplied with 2% w/v of sarkosyl and incubated for 20 minutes at 37 ^{o}C. The sample was centrifuged for 10 minutes at 20000xg, and 25 ^{o}C. The supernatant was

ultracentrifuged for 20 minutes at 100000xg and 25 °C. The pellet was resuspended in 750 µl/1g starting material of 10 mM TRIS-HCl pH 7.5, 1 mM EGTA, 0.8 M NaCl, 10% sucrose, and centrifuged at 9800xg for 20 minutes. The supernatant was ultracentrifuged for 1 hour at 100000xg. The pellet was resuspended in 25 µl/g starting material of 20 mM TRIS-HCl pH 7.4, 100 mM NaCl, and stored at 4 °C up to a month. Presence of CBD fibrils was assessed by TEM.

Microscale thermophoresis binding assay

Binding between FibrilPaint1 or FibrilPaint6 and CHIP was analyzed using Monolith (NanoTemper Technologies) Microscale thermophoresis system (MST). Thermophoresis was monitored at a concentration of 50 nM of FibrilPaint and a dilution series of CHIP, in 25 mM HEPES-KOH pH 7.5, 75 mM KCl, 75 mM NaCl. Samples were transferred to premium capillaries (NanoTemper Technologies) and measurements were performed at 37 °C, with medium blue LED power and at MST infrared laser power of 50% to induce thermophoretic motion. The infrared laser was switched on 1 s after the start of the measurement for a 20 s period. Datapoints used were the MST response at 5 seconds.

Ubiquitination of amyloid fibrils

For the ubiquitination reaction, enzymes were diluted into ubiquitination buffer (40mM TRIS pH = 8, 5 mM MgCl2, 0.05% TWEEN-20 and 1 mM DTT) to a final concentration of 500 nM E1, 500 nM E2, 500 nM E3, 10 nM Fluorescein-Ubiquitin, 500 nM FibrilPaint, 5 µM fibrils, and in presence or absence of 5 mM ATP. The reaction was then incubated for 1 h at 30 °C. To determine ubiquitination, sample was loaded onto FIDA1 with a 480 nm excitation source. The mode of operation use is capillary dissociation (Capdis). In this, the capillary is equilibrated with buffer followed by injection of the sample (Table 2).

Table 2. Experimental parameters for Capdis analysis of protein fibril size up to a R_h of 75 nm.

Tray	Vial	Pressure (mbar)	Time (s)	Outlet	Measure	Comments
2	1	3500	45	Variable	No	1 M NaOH
2	2	3500	75	Variable	No	Buffer equilibration
1	Analyte	3500	20	Variable	No	Buffer

1	Indicator	50	10	Variable	No	Sample application
1	Analyte	75	1800	Variable	Yes	Buffer

Tray 1 was maintained at 37 °C and tray 2 and capillary chamber at 25 °C

5. Acknowledgements

SGDR was supported by grants of the Campaign Team Huntington and Alzheimer Nederland (No. WE.03-2019-03) and a ZonMW TOP grant (No. 91215084). AF thanks The Minerva Center for Bio-Hybrid complex systems and the Saerree K. and Louis P. Fiedler Chair in Chemistry. Measurements on the FIDA1, CLARIOstar® Plus and Monolith were done at the Protein Research Centre of Utrecht University. We are grateful to xxx for their contribution to the experimental work of this research.

6. Conflict of interest

JAP, FAD, GM, AF and SGDR are named as inventors in a patent (EP23194706, 'Peptides for the detection of amyloid fibril Aggregates') filed by Universiteit Utrecht Holding BV describing the peptides mentioned in this manuscript. The other authors declare no competing interests.

7. Author contributions

Conception FAD, JAP, SGDR

Design of the work JAP, FAD, SGDR

Acquisition JAP, FAD, APR, GH

Analysis FAD, JAP

Interpretation of data JAP, FAD, SGDR

Writing original draft FAD

Revision FAD, JAP, SGDR

6. References

- [1] B.N. Dugger, D.W. Dickson, Pathology of Neurodegenerative Diseases, Cold Spring Harb. Perspect. Biol. 9 (2017) a028035.
- [2] D.S. Knopman, H. Amieva, R.C. Petersen, G. Chételat, D.M. Holtzman, B.T. Hyman, R.A. Nixon, D.T. Jones, Alzheimer disease, Nature Reviews Disease Primers 7 (2021) 33.
- [3] D. Aarsland, L. Batzu, G.M. Halliday, G.J. Geurtsen, C. Ballard, K. Ray Chaudhuri, D. Weintraub, Parkinson disease-associated cognitive impairment, Nature Reviews Disease Primers 7 (2021) 47.
- [4] S.J. Tabrizi, M.D. Flower, C.A. Ross, E.J. Wild, Huntington disease: new insights into molecular pathogenesis and therapeutic opportunities, Nature Reviews Neurology 16 (2020) 529-546.
- [5] M. DiFiglia, E. Sapp, K.O. Chase, S.W. Davies, G.P. Bates, J.P. Vonsattel, N. Aronin, Aggregation of huntingtin in neuronal intranuclear inclusions and dystrophic neurites in brain, Science (New York, N.Y.) 277 (1997) 1990-1993.
- [6] F.R. Buccellato, M. D'Anca, G.M. Tartaglia, M. Del Fabbro, E. Scarpini, D. Galimberti, Treatment of Alzheimer's Disease: Beyond Symptomatic Therapies, Int J Mol Sci 24 (2023).
- [7] S. Chowdhury, N.S. Chowdhury, Novel anti-amyloid-beta (Aβ) monoclonal antibody lecanemab for Alzheimer's disease: A systematic review, Int. J. Immunopathol. Pharmacol. 37 (2023) 3946320231209839.
- [8] S. Cohen, C.H. van Dyck, M. Gee, T. Doherty, M. Kanekiyo, S. Dhadda, D. Li, S. Hersch, M. Irizarry, L.D. Kramer, Lecanemab Clarity AD: Quality-of-Life Results from a Randomized, Double-Blind Phase 3 Trial in Early Alzheimer's Disease, J Prev Alzheimers Dis 10 (2023) 771-777.
- [9] C.H. Van Dyck, C.J. Swanson, P. Aisen, R.J. Bateman, C. Chen, M. Gee, M. Kanekiyo, D. Li, L. Reyderman, S. Cohen, L. Froelich, S. Katayama, M. Sabbagh, B. Vellas, D. Watson, S. Dhadda, M. Irizarry, L.D. Kramer, T. Iwatsubo, Lecanemab in Early Alzheimer’s Disease, New England Journal of Medicine 388 (2023) 9-21.
- [10] S. Kuemper, A.G. Cairns, K. Birchall, Z. Yao, J.M. Large, Targeted protein degradation in CNS disorders: a promising route to novel therapeutics?, Front Mol Neurosci 17 (2024) 1370509.
- [11] S.H. Scheres, M. Goedert, Molecular pathology of neurodegenerative diseases by cryo-EM of amyloids., Nature 621(7980) (2023) 701-710. .
- [12] E.H. Koo, P.T. Lansbury, J.W. Kelly, Amyloid diseases: Abnormal protein aggregation in neurodegeneration, Proceedings of the National Academy of Sciences 96 (1999) 9989-9990.
- [13] G.K. Wilcock, M.M. Esiri, Plaques, tangles and dementia. A quantitative study, J. Neurol. Sci. 56 (1982) 343-356.
- [14] A. Bejanin, D.R. Schonhaut, R. La Joie, J.H. Kramer, S.L. Baker, N. Sosa, N. Ayakta, A. Cantwell, M. Janabi, M. Lauriola, J.P. O'Neil, M.L. Gorno-Tempini, Z.A. Miller, H.J. Rosen, B.L. Miller, W.J. Jagust, G.D. Rabinovici, Tau pathology and neurodegeneration contribute to cognitive impairment in Alzheimer's disease, Brain : a journal of neurology 140 (2017) 3286-3300.
- [15] C. Ballatore, V.M. Lee, J.Q. Trojanowski, Tau-mediated neurodegeneration in Alzheimer's disease and related disorders, Nature reviews.Neuroscience 8 (2007) 663-672.
- [16] M.H. Polymeropoulos, C. Lavedan, E. Leroy, S.E. Ide, A. Dehejia, A. Dutra, B. Pike, H. Root, J. Rubenstein, R. Boyer, E.S. Stenroos, S. Chandrasekharappa, A. Athanassiadou, T. Papapetropoulos, W.G. Johnson, A.M. Lazzarini, R.C. Duvoisin, G. Di Iorio, L.I. Golbe, R.L. Nussbaum, Mutation in the alpha-synuclein gene identified in families with Parkinson's disease, Science (New York, N.Y.) 276 (1997) 2045-2047.
- [17] Y. Ihara, N. Nukina, R. Miura, M. Ogawara, Phosphorylated tau protein is integrated into paired helical filaments in Alzheimer's disease, J. Biochem. 99 (1986) 1807-1810.
- [18] S.S. Sisodia, D.L. Price, Role of the β-amyloid protein in Alzheimer's disease, The FASEB Journal 9 (1995) 366-370.

- [19] M.B. Koopman, L. Ferrari, S.G.D. Rüdiger, How do protein aggregates escape quality control in neurodegeneration?, Trends Neurosci. 45 (2022) 257-271.
- [20] R.E. Lackie, A. Maciejewski, V.G. Ostapchenko, J. Marques-Lopes, W.Y. Choy, M.L. Duennwald, V.F. Prado, M.A.M. Prado, The Hsp70/Hsp90 Chaperone Machinery in Neurodegenerative Diseases, Frontiers in neuroscience 11 (2017) 254.
- [21] B. Bukau, J. Weissman, A. Horwich, Molecular chaperones and protein quality control, Cell 125 (2006) 443-451.
- [22] W.E. Balch, R.I. Morimoto, A. Dillin, J.W. Kelly, Adapting proteostasis for disease intervention, Science (New York, N.Y.) 319 (2008) 916-919.
- [23] J. Labbadia, R.I. Morimoto, The biology of proteostasis in aging and disease, Annu. Rev. Biochem. 84 (2015) 435-464.
- [24] X. Wang, Z.-L. Qin, N. Li, M.-Q. Jia, Q.-G. Liu, Y.-R. Bai, J. Song, S. Yuan, S.-Y. Zhang, Annual review of PROTAC degraders as anticancer agents in 2022, European Journal of Medicinal Chemistry 267 (2024) 116166.
- [25] Y. Liu, J. Yang, T. Wang, M. Luo, Y. Chen, C. Chen, Z.e. Ronai, Y. Zhou, E. Ruppin, L. Han, Expanding PROTACtable genome universe of E3 ligases, Nature Communications 14 (2023) 6509.
- [26] M. Békés, D.R. Langley, C.M. Crews, PROTAC targeted protein degraders: the past is prologue, Nature Reviews Drug Discovery 21 (2022) 181-200.
- [27] K.M. Sakamoto, K.B. Kim, A. Kumagai, F. Mercurio, C.M. Crews, R.J. Deshaies, Protacs: chimeric molecules that target proteins to the Skp1-Cullin-F box complex for ubiquitination and degradation, Proceedings of the National Academy of Sciences of the United States of America 98 (2001) 8554-8559.
- [28] M. Campone, C.X. Ma, M.D. Laurentiis, H. Iwata, S.A. Hurvitz, S.A. Wander, M.A. Danso, D.R. Lu, J.P. Smith, Y. Liu, L. Tran, S. Anderson, E.P. Hamilton, VERITAC-2: A global, randomized phase 3 study of ARV-471, a proteolysis targeting chimera (PROTAC) estrogen receptor (ER) degrader, vs fulvestrant in ER+/human epidermal growth factor receptor 2 (HER2)- advanced breast cancer, Journal of Clinical Oncology 41 (2023) TPS1122-TPS1122.
- [29] J. Aragonès Pedrola, F.A. Dekker, K. Guttmann, L.M. van Leeuwen, S. Singh, G. Mayer, T. Garfagnini, A. Friedler, S.G.D. Rudiger, Fibril Paint: a class of amyloid-targeting peptides, bioRxiv (2024) 2024.08.25.609586.
- [30] J. Aragonès Pedrola, F. Dekker, A., T. Garfagnini, G. Mayer, M. Koopman, B., M. Bergmeijer, F. Förster, J. Hoozemans, J. M., H. Jensen, A. Friedler, S. Rüdiger, G. D., Fibril Paint to detect Amyloids and determine Fibril Length, BioRxiv (2023).
- [31] T. Garfagnini, L. Ferrari, M.B. Koopman, S. Halters, E. Van Kappel, G. Mayer, M.M. Maurice, S.G.D. Rüdiger, A. Friedler, A peptide strategy for inhibiting different protein aggregation pathways in disease, bioRxiv (2022) 2022.10.22.513060.
- [32] C.A. Ballinger, P. Connell, Y. Wu, Z. Hu, L.J. Thompson, L.Y. Yin, C. Patterson, Identification of CHIP, a novel tetratricopeptide repeat-containing protein that interacts with heat shock proteins and negatively regulates chaperone functions, Mol. Cell. Biol. 19 (1999) 4535-4545.
- [33] P. Connell, C.A. Ballinger, J. Jiang, Y. Wu, L.J. Thompson, J. Hohfeld, C. Patterson, The co-chaperone CHIP regulates protein triage decisions mediated by heat-shock proteins, Nat. Cell Biol. 3 (2001) 93-96.
- [34] V.A. Assimon, D.R. Southworth, J.E. Gestwicki, Specific Binding of Tetratricopeptide Repeat Proteins to Heat Shock Protein 70 (Hsp70) and Heat Shock Protein 90 (Hsp90) Is Regulated by Affinity and Phosphorylation, Biochemistry 54 (2015) 7120-7131.
- [35] C.A. Dickey, J. Koren, Y.J. Zhang, Y.F. Xu, U.K. Jinwal, M.J. Birnbaum, B. Monks, M. Sun, J.Q. Cheng, C. Patterson, R.M. Bailey, J. Dunmore, S. Soresh, C. Leon, D. Morgan, L. Petrucelli, Akt and CHIP

coregulate tau degradation through coordinated interactions, Proc. Natl. Acad. Sci. USA 105 (2008) 3622-3627.

- [36] L. Petrucelli, D. Dickson, K. Kehoe, J. Taylor, H. Snyder, A. Grover, M. De Lucia, E. McGowan, J. Lewis, G. Prihar, J. Kim, W.H. Dillmann, S.E. Browne, A. Hall, R. Voellmy, Y. Tsuboi, T.M. Dawson, B. Wolozin, J. Hardy, M. Hutton, CHIP and Hsp70 regulate tau ubiquitination, degradation and aggregation, Hum. Mol. Genet. 13 (2004) 703-714.
- [37] M.B. Koopman, S.G.D. Rüdiger, Alzheimer Cells on Their Way to Derailment Show Selective Changes in Protein Quality Control Network, Front. Mol. Biosci. 7 (2020) 214.
- [38] H. Jensen, J. Østergaard, Flow induced dispersion analysis quantifies noncovalent interactions in nanoliter samples, JACS 132 (2010) 4070-4071.
- [39] M.E. Pedersen, J. Østergaard, H. Jensen, Flow-Induced Dispersion Analysis (FIDA) for Protein Quantification and Characterization, in: T.M. Phillips (Ed.), Clinical Applications of Capillary Electrophoresis: Methods and Protocols, Springer New York, New York, NY, 2019, pp. 109-123.
- [40] J. Lowe, A. Blanchard, K. Morrell, G. Lennox, L. Reynolds, M. Billett, M. Landon, R.J. Mayer, Ubiquitin is a common factor in intermediate filament inclusion bodies of diverse type in man, including those of Parkinson's disease, Pick's disease, and Alzheimer's disease, as well as Rosenthal fibres in cerebellar astrocytomas, cytoplasmic bodies in muscle, and mallory bodies in alcoholic liver disease, The Journal of pathology 155 (1988) 9-15.
- [41] A. Pilon, P. Yost, T.E. Chase, G. Lohnas, T. Burkett, S. Roberts, W.E. Bentley, Ubiquitin fusion technology: bioprocessing of peptides, Biotechnology progress 13 (1997) 374-379.
- [42] S. Vijay-Kumar, C.E. Bugg, W.J. Cook, Structure of ubiquitin refined at 1.8 A resolution, J. Mol. Biol. 194 (1987) 531-44.
- [43] Z. Lv, K.M. Williams, L. Yuan, J.H. Atkison, S.K. Olsen, Crystal structure of a human ubiquitin E1-ubiquitin complex reveals conserved functional elements essential for activity, J. Biol. Chem. 293 (2018) 18337-18352.
- [44] A. Pichler, P. Knipscheer, E. Oberhofer, W.J. van Dijk, R. Körner, J.V. Olsen, S. Jentsch, F. Melchior, T.K. Sixma, SUMO modification of the ubiquitin-conjugating enzyme E2-25K, Nat. Struct. Mol. Biol. 12 (2005) 264-9.
- [45] A.J. Middleton, C.L. Day, The molecular basis of lysine 48 ubiquitin chain synthesis by Ube2K, Sci Rep 5 (2015) 16793.
- [46] M. Zhang, M. Windheim, S.M. Roe, M. Peggie, P. Cohen, C. Prodromou, L.H. Pearl, Chaperoned ubiquitylation--crystal structures of the CHIP U box E3 ubiquitin ligase and a CHIP-Ubc13-Uev1a complex, Mol. Cell 20 (2005) 525-538.
- [47] D. Hagemans, I.A.M. van Belzen, T. Morán Luengo, S.G.D. Rüdiger, A script to highlight hydrophobicity and charge on protein surfaces, Front. Mol. Biosci. 2 (2015) 56.
- [48] Y. Shi, W. Zhang, Y. Yang, A.G. Murzin, B. Falcon, A. Kotecha, M. van Beers, A. Tarutani, F. Kametani, H.J. Garringer, R. Vidal, G.I. Hallinan, T. Lashley, Y. Saito, S. Murayama, M. Yoshida, H. Tanaka, A. Kakita, T. Ikeuchi, A.C. Robinson, D.M.A. Mann, G.G. Kovacs, T. Revesz, B. Ghetti, M. Hasegawa, M. Goedert, S.H.W. Scheres, Structure-based classification of tauopathies, Nature 598 (2021) 359-363.
- [49] M.M. Mocanu, A. Nissen, K. Eckermann, I. Khlistunova, J. Biernat, D. Drexler, O. Petrova, K. Schonig, H. Bujard, E. Mandelkow, L. Zhou, G. Rune, E.M. Mandelkow, The potential for beta-structure in the repeat domain of Tau protein determines aggregation, synaptic decay, neuronal loss, and coassembly with endogenous Tau in inducible mouse models of tauopathy, J. Neurosci. 28 (2008) 737-748.
- [50] P. McColgan, S.J. Tabrizi, Huntington's disease: a clinical review, European journal of neurology 25 (2018) 24-34.
- [51] F. Saudou, S. Humbert, The Biology of Huntingtin, Neuron 89 (2016) 910-926.
- [52] E. Tolosa, G. Wenning, W. Poewe, The diagnosis of Parkinson's disease, The Lancet Neurology 5 (2006) 75-86.

○ [53] J. Hardy, D.J. Selkoe, The amyloid hypothesis of Alzheimer's disease: progress and problems on the road to therapeutics, Science (New York, N.Y.) 297 (2002) 353-356.
○ [54] C.R. Jack Jr., J.S. Andrews, T.G. Beach, T. Buracchio, B. Dunn, A. Graf, O. Hansson, C. Ho, W. Jagust, E. McDade, J.L. Molinuevo, O.C. Okonkwo, L. Pani, M.S. Rafii, P. Scheltens, E. Siemers, H.M. Snyder, R. Sperling, C.E. Teunissen, M.C. Carrillo, Revised criteria for diagnosis and staging of Alzheimer's disease: Alzheimer's Association Workgroup, Alzheimers. Dement. (2024).
○ [55] G.S. Bloom, Amyloid-beta and tau: the trigger and bullet in Alzheimer disease pathogenesis, JAMA neurology 71 (2014) 505-508.
○ [56] B.M. Helabad, I. Matlahov, J.O. Daldrop, G. Jain, P.C.A. van der Wel, M.S. Miettinen, Integrative determination of the atomic structure of mutant huntingtin exon 1 fibrils from Huntington's disease, bioRxiv (2023).
○ [57] J.C. Boatz, T. Piretra, A. Lasorsa, I. Matlahov, J.F. Conway, P.C.A. van der Wel, Protofilament Structure and Supramolecular Polymorphism of Aggregated Mutant Huntingtin Exon 1, J. Mol. Biol. 432 (2020) 4722-4744.
○ [58] A.W.P. Fitzpatrick, B. Falcon, S. He, A.G. Murzin, G. Murshudov, H.J. Garringer, R.A. Crowther, B. Ghetti, M. Goedert, S.H.W. Scheres, Cryo-EM structures of tau filaments from Alzheimer's disease, Nature 547 (2017) 185-190.
○ [59] W. Zhang, B. Falcon, A.G. Murzin, J. Fan, R.A. Crowther, M. Goedert, S.H. Scheres, Heparin-induced tau filaments are polymorphic and differ from those in Alzheimer's and Pick's diseases, eLife 8 (2019) 10.7554/eLife.43584.
○ [60] S. Lövestam, D. Li, J.L. Wagstaff, A. Kotecha, D. Kimanius, S.H. McLaughlin, A.G. Murzin, S.M. Freund, M. Goedert, S.H. Scheres, Disease-specific tau filaments assemble via polymorphic intermediates, Nature 625(7993) (2024) 119-125.
○ [61] S.H. Scheres, M. Goedert, Molecular pathology of neurodegenerative diseases by cryo-EM of amyloids., Nature 621(7980) (2023) 701-710.
○ [62] B. Falcon, W. Zhang, A.G. Murzin, G. Murshudov, H.J. Garringer, R. Vidal, R.A. Crowther, B. Ghetti, S.H.W. Scheres, M. Goedert, Structures of filaments from Pick's disease reveal a novel tau protein fold, Nature 561 (2018) 137-140.
○ [63] W. Zhang, A. Tarutani, K.L. Newell, A.G. Murzin, T. Matsubara, B. Falcon, R. Vidal, H.J. Garringer, Y. Shi, T. Ikeuchi, S. Murayama, B. Ghetti, M. Hasegawa, M. Goedert, S.H.W. Scheres, Novel tau filament fold in corticobasal degeneration, Nature 580 (2020) 283-287.
○ [64] I. Dikic, Proteasomal and Autophagic Degradation Systems, Annu. Rev. Biochem. 86 (2017) 193-224.
○ [65] I. Dikic, Proteasomal and Autophagic Degradation Systems, Annu. Rev. Biochem. 86 (2017) 193-224.
○ [66] Y. Yang, D. Arseni, W. Zhang, M. Huang, S. Lövestam, M. Schweighauser, A. Kotecha, A.G. Murzin, S.Y. Peak-Chew, J. Macdonald, I. Lavenir, H.J. Garringer, E. Gelpi, K.L. Newell, G.G. Kovacs, R. Vidal, B. Ghetti, B. Ryskeldi-Falcon, S.H.W. Scheres, M. Goedert, Cryo-EM structures of amyloid-β 42 filaments from human brains, Science (New York, N.Y.) 375 (2022) 167-172.
○ [67] Y. Yang, Y. Shi, M. Schweighauser, X. Zhang, A. Kotecha, A.G. Murzin, H.J. Garringer, P.W. Cullinane, Y. Saito, T. Foroud, T.T. Warner, K. Hasegawa, R. Vidal, S. Murayama, T. Revesz, B. Ghetti, M. Hasegawa, T. Lashley, S.H.W. Scheres, M. Goedert, Structures of α-synuclein filaments from human brains with Lewy pathology, Nature 610 (2022) 791-795.
○ [68] S.H. Scheres, W. Zhang, B. Falcon, M. Goedert, Cryo-EM structures of tau filaments, Curr. Opin. Struct. Biol. 64 (2020) 17-25.
○ [69] B. Falcon, J. Zivanov, W. Zhang, A.G. Murzin, H.J. Garringer, R. Vidal, R.A. Crowther, K.L. Newell, B. Ghetti, M. Goedert, S.H.W. Scheres, Novel tau filament fold in chronic traumatic encephalopathy encloses hydrophobic molecules, Nature 568 (2019) 420-423.

○ [70] M. Wilkinson, Y. Xu, D. Thacker, A.I.P. Taylor, D.G. Fisher, R.U. Gallardo, S.E. Radford, N.A. Ranson, Structural evolution of fibril polymorphs during amyloid assembly, Cell 186 (2023) 5798–5811.
○ [71] Y. Fang, J. Wang, M. Zhao, Q. Zheng, C. Ren, Y. Wang, J. Zhang, Progress and Challenges in Targeted Protein Degradation for Neurodegenerative Disease Therapy, J. Med. Chem. 65 (2022) 11454-11477.
○ [72] W. Wang, Q. Zhou, T. Jiang, S. Li, J. Ye, J. Zheng, X. Wang, Y. Liu, M. Deng, D. Ke, Q. Wang, Y. Wang, J.Z. Wang, A novel small-molecule PROTAC selectively promotes tau clearance to improve cognitive functions in Alzheimer-like models, Theranostics 11 (2021) 5279-5295.
○ [73] H. Inuzuka, J. Liu, W. Wei, A.H. Rezaeian, PROTACs technology for treatment of Alzheimer's disease: Advances and perspectives, Acta Mater Med 1 (2022) 24-41.
○ [74] M.C. Silva, F.M. Ferguson, Q. Cai, K.A. Donovan, G. Nandi, D. Patnaik, T. Zhang, H.-T. Huang, D.E. Lucente, B.C. Dickerson, T.J. Mitchison, E.S. Fischer, N.S. Gray, S.J. Haggarty, Targeted degradation of aberrant tau in frontotemporal dementia patient-derived neuronal cell models, eLife 8 (2019) e45457.
○ [75] C.A. Dickey, A. Kamal, K. Lundgren, N. Klosak, R.M. Bailey, J. Dunmore, P. Ash, S. Shoraka, J. Zlatkovic, C.B. Eckman, C. Patterson, D.W. Dickson, N.S.N. Jr, M. Hutton, F. Burrows, L. Petrucelli, The high-affinity HSP90-CHIP complex recognizes and selectively degrades phosphorylated tau client proteins, J. Clin. Investig. 117 (2007) 648-658.
○ [76] S. Tomoshige, S. Nomura, K. Ohgane, Y. Hashimoto, M. Ishikawa, Discovery of Small Molecules that Induce the Degradation of Huntingtin, Angewandte Chemie (International ed.in English) 56 (2017) 11530-11533.
○ [77] S. Tomoshige, S. Nomura, K. Ohgane, Y. Hashimoto, M. Ishikawa, Degradation of huntingtin mediated by a hybrid molecule composed of IAP antagonist linked to phenyldiazenyl benzothiazole derivative, Bioorganic & Medicinal Chemistry Letters 28 (2018) 707-710.
○ [78] O.D. Jarosińska, S.G.D. Rüdiger, Molecular Strategies to Target Protein Aggregation in Huntington's Disease, Front. Mol. Biosci. 8 (2021) 769184.
○ [79] J. Lee, K.W. Sung, E.-J. Bae, D. Yoon, D. Kim, J.S. Lee, D.-h. Park, D.Y. Park, S.R. Mun, S.C. Kwon, Targeted degradation ofα-synuclein aggregates in Parkinson's disease using the AUTOTAC technology, Molecular neurodegeneration 18 (2023) 41.
○ [80] C.H. Ji, H.Y. Kim, M.J. Lee, A.J. Heo, D.Y. Park, S. Lim, S. Shin, W.S. Yang, C.A. Jung, K.Y. Kim, E.H. Jeong, S.H. Park, S. Bin Kim, S.J. Lee, J.E. Na, J.I. Kang, H.M. Chi, H.T. Kim, Y.K. Kim, B.Y. Kim, Y.T. Kwon, The AUTOTAC chemical biology platform for targeted protein degradation via the autophagy-lysosome system, Nat. Commun. 13 (2022) 904-4.
○ [81] K. Cassidy, H. Zhao, Redefining the Scope of Targeted Protein Degradation: Translational Opportunities in Hijacking the Autophagy-Lysosome Pathway, Biochemistry (2021).
○ [82] M. Kocak, S. Ezazi Erdi, G. Jorba, I. Maestro, J. Farrés, V. Kirkin, A. Martinez, O. Pless, Targeting autophagy in disease: established and new strategies, Autophagy (2021) 1-23.
○ [83] D. Takahashi, H. Arimoto, Selective autophagy as the basis of autophagy-based degraders, Cell chemical biology 28 (2021) 1061-1071.
○ [84] D. Takahashi, J. Moriyama, T. Nakamura, E. Miki, E. Takahashi, A. Sato, T. Akaike, K. Itto-Nakama, H. Arimoto, AUTACs: Cargo-Specific Degraders Using Selective Autophagy, Mol. Cell 76 (2019) 797-810.e10.
○ [85] T.A. Thibaudeau, R.T. Anderson, D.M. Smith, A common mechanism of proteasome impairment by neurodegenerative disease-associated oligomers, Nat. Commun. 9 (2018) 1097-0.
○ [86] K. Gauthreaux, T.A. Bonnett, L.M. Besser, W.D. Brenowitz, M. Teylan, C. Mock, Y.C. Chen, K.C.G. Chan, C.D. Keene, X.H. Zhou, W.A. Kukull, Concordance of Clinical Alzheimer Diagnosis and Neuropathological Features at Autopsy, J. Neuropathol. Exp. Neurol. 79 (2020) 465-473.
○ [87] J. Rahimi, G.G. Kovacs, Prevalence of mixed pathologies in the aging brain, Alzheimers Res Ther 6 (2014) 82.

○ [88] A. Kapasi, C. DeCarli, J.A. Schneider, Impact of multiple pathologies on the threshold for clinically overt dementia, Acta Neuropathol 134 (2017) 171-186.